RSC Advances

PAPER

View Article Online
View Journal | View Issue

Cite this: *RSC Adv.*, 2021, **11**, 10996

In situ hydrodeoxygenation of vanillin over Ni–Co–P/HAP with formic acid as a hydrogen source

Mingxing Duan, Qingyan Cheng,* Mingming Wang and Yanji Wang

A new noble metal-free Ni–Co–P/HAP (hydroxyapatite) amorphous alloy catalyst was synthesized by an impregnation-chemical reduction method; the structure and properties of the catalysts were characterized by XRD, SEM, BET, XPS and DSC. Based on the model of the hydrodeoxygenation (HDO) of vanillin to 2-methoxy-4-methylphenol (MMP) with formic acid as a hydrogen source, the catalytic performance of the catalyst was studied. The results found that the Ni–Co–P/HAP catalyst exhibited excellent catalytic activity for the *in situ* HDO reaction of vanillin compared with Ni–P and Ni–Co–P. The conversion of vanillin could be high to 97.86% with MMP selectivity of 93.97% under optimized reaction conditions. In addition, mechanism studies have shown that the side reaction of carbocation and vanillyl alcohol (HMP) condensation can be effectively reduced with increasing the hydrogenation rate, thereby the selectivity of MMP was effectively increased.

Received 5th February 2021
Accepted 3rd March 2021

DOI: 10.1039/d1ra00979f

rsc.li/rsc-advances

Introduction

With the rapid increase of the global population, the consumption of petrochemical resources has become increasingly serious, the energy demand has risen rapidly, and the supply of fossil fuels is insufficient, which makes the development of new energy sources imminent.[1,2] The pyrolysis of lignocellulosic biomass is a prospective approach for producing valuable liquid biomass oil. As an effective strategy, hydrodeoxygenation (HDO) is of vital importance for improving the energy density of bio-oil by selectively removing oxygen-containing groups.[3,4] The traditional HDO technology requires explosive fossil resource-derived hydrogen gas that is dangerous and uncontrollable, often leading to excessive hydrogenation and C–C cleavage.[5,6] Studies have found that as a new type of hydrogen storage material, formic acid has good stability, is easy to store and transport, and has a large hydrogen capacity, and has been widely used as a hydrogen source in hydrogenation reactions.[7–10]

In recent years, supported precious metal catalysts have been used for the decomposition of formic acid and the hydrodeoxygenation of biomass oil. 2-Methoxy-4-methylphenol (MMP) is an important intermediate for medicine and perfume, which can be obtained by the hydrodeoxygenation of vanillin. Meanwhile, the HDO reaction of vanillin was often used as a probe reaction to investigate the hydrogenation performance of the catalyst.[11–13] Nie R. *et al.*[14] studied the HDO reaction of vanillin and found that the vanillin conversion and the selectivity of the product 2-methoxy-4-methylphenol (MMP) were both above 90% with N-doped carbon-supported Pd as the catalyst and formic acid as a hydrogen donor. Although noble metal catalysts have a good catalytic effect on biomass oil HDO, the low reserves and high cost of noble metals limit its large-scale industrial production. Nickel-based amorphous alloy catalysts have received widespread attention because of their low price, simple preparation process, and excellent catalytic performance in the HDO reaction of vanillin.[15,16] Brandi *et al.*[17] synthesized a stable Ni catalyst and loaded it on nitrogen-doped carbon (NDC). The catalytic performance of the catalyst was evaluated in the aqueous hydrogenation reaction of vanillin. Studies have found that the Ni/NDC catalyst exhibits high catalytic performance in the aqueous hydrogenation of vanillin with hydrogen as the hydrogen source, and the conversion of vanillin and the selectivity of product MMP are close to 100%.

Although Ni-based amorphous alloy catalysts have exhibited excellent catalytic activity in the hydrogenation reactions, it still has problems with small specific surface area, easy agglomeration, and poor thermal stability, *etc.* Studies have shown that the degree of disorder of the Ni-based amorphous alloy can be increased and the agglomeration of the catalyst can be reduced by introducing the transition metal Co. Meanwhile, as a material with high reserves, low cost and high activity, phosphorus can form a chelated structure with nickel in Ni–Co–P amorphous alloy, thereby improving the stability of the catalyst. There is a large difference between the size of P atom and transition metal Ni, Co atom. The defect sites of the catalyst can be easily produced when P was incorporated into the material

School of Chemical Engineering, Hebei University of Technology, Key Laboratory of Green Chemical Technology and High Efficient Energy Saving of Hebei Province, Tianjin Key Laboratory of Chemical Process Safety, Tianjin, 300130, China. E-mail: chengqingyan@hebut.edu.cn

structure framework, which is beneficial to the formation of amorphous alloy structure. In addition, the specific surface area and stability of the catalyst can be improved by supporting the amorphous alloy on the carrier, which enables the activity of the catalyst to be improved. Among many carriers, HAP was widely used as a catalyst carrier due to its mesoporous structure, large specific surface area, high porosity and good thermal stability. Moreover, although Ni-based amorphous alloy catalysts have good catalytic performance in HDO reactions using hydrogen as the hydrogen source, there are few reports on the use of formic acid as the hydrogen source. Therefore, it is of great significance for the purification of biomass oil and large-scale industrial production through the development of cheap, efficient, and stable Ni-based amorphous alloy catalysts to catalyze the decomposition of formic acid to produce hydrogen and further catalyze the HDO reaction of vanillin.

In this work, the Ni–Co–P/HAP (hydroxyapatite) amorphous alloy catalyst was prepared by the impregnation-chemical reduction method. The catalytic performance of Ni–Co–P/HAP in the *in situ* HDO reaction of vanillin was studied with formic acid as the hydrogen source, which provides a new method for the refining of biomass oil. Meanwhile, the effect of hydrogen protons on the selectivity of MMP was studied, the mechanism of the vanillin HDO reaction catalyzed by Ni–Co–P/HAP with formic acid as the hydrogen source was proposed.

Experimental

Materials

$NiCl_2 \cdot 6H_2O$, $Co(NO_3)_2 \cdot 6H_2O$, $NaH_2PO_2 \cdot H_2O$, KBH_4 and 25 wt% $NH_3 \cdot H_2O$ were purchased from Sailboat Chemical Reagent Technology Co., Ltd. (Tianjin, China). Vanillin, vanillyl alcohol (HMP), 2-methoxy-4-methylphenol (MMP) and hydroxyapatite ($Ca_{10}(PO_4)_6(OH)_2$, HAP) were purchased from Aladdin Biochemical Technology Co., Ltd. (Shanghai, China). $CH_3COONa \cdot 3H_2O$, ethanol and isopropanol were purchased from Reagent No. 1 Factory (Tianjin, China). N_2 was purchased from Sizhi Gas Co., Ltd. (99.999%, Tianjin, China). All chemicals are analytical pure and used as received without further purification.

Synthesis of Ni–P and Ni–Co–P amorphous alloys

The Ni–P and Ni–Co–P amorphous alloys were prepared by the chemical reduction method. $NiCl_2 \cdot 6H_2O$ (2.5 mmol, 0.5942 g), $NaH_2PO_2 \cdot H_2O$ (20 mmol, 1.060 g), $CH_3COONa \cdot 3H_2O$ (1.25 mmol, 0.1701 g) and deionized water (30 mL) were added to the three-necked flask, adjusted the pH of the solution to 9.0 with 25 wt% $NH_3 \cdot H_2O$ at 30 °C. Under the protection of N_2, a few drops of KBH_4 solution (3 mol L^{-1}) were added dropwise to the solution to induce the reaction to occur, during which a black precipitate was formed and accompanied by bubbles. The reaction was carried out at 30 °C for a certain period of time, and the reaction was stopped when no bubbles are formed. The product was separated by centrifugation, washed with deionized water to neutrality, washed with anhydrous ethanol three times, and dried in vacuum at 50 °C for 8 h to obtain a Ni–P amorphous alloy catalyst. The preparation process of Ni–Co–P amorphous alloy is similar to the above process. $NiCl_2 \cdot 6H_2O$ (2.5 mmol, 0.5942 g), $NaH_2PO_2 \cdot H_2O$ (20 mmol, 1.060 g), $CH_3COONa \cdot 3H_2O$ (1.25 mmol, 0.1701 g), $Co(NO_3)_2 \cdot 6H_2O$ (2 mmol, 0.5821 g) and deionized water (30 mL) were added to a 150 mL three-necked flask, the other steps are the same as the preparation of Ni–P amorphous alloy catalyst.

Synthesis of supported Ni–Co–P/HAP amorphous alloy

The Ni–Co–P/HAP amorphous alloy was prepared by impregnation-chemical reduction method. $NiCl_2 \cdot 6H_2O$ (2.5 mmol, 0.5942 g), $NaH_2PO_2 \cdot H_2O$ (20 mmol, 1.060 g), $CH_3COONa \cdot 3H_2O$ (1.25 mmol, 0.1701 g), $Co(NO_3)_2 \cdot 6H_2O$ (2 mmol, 0.5821 g) and deionized water (30 mL) were added to the three-necked flask, adjusted the pH of solution to 9.0 with 25 wt% $NH_3 \cdot H_2O$, followed by HAP (0.3 g) was added to the above solution. The reaction solution was magnetically stirred at room temperature for 12 h. Then, a few drops of KBH_4 solution (3 mol L^{-1}) were added slowly to the above solution to induce the reaction to occur. The reaction was carried out at 30 °C for a certain period of time, and the reaction was stopped when no bubbles are formed. The product was separated by centrifugation, washed with deionized water to neutrality, then washed with anhydrous ethanol three times, and vacuum dried at 50 °C for 8 h to obtain Ni–Co–P/HAP amorphous alloy.

Catalyst characterization

Powder X-ray diffraction (XRD) patterns were recorded on a D/MAX-2500 X-ray diffractometer from Nippon Science, Inc., with Cu Kα rays at a scan rate of 8° min^{-1}, tube voltage and current of 40 kV and 100 mA respectively, and a scan range of 20–70°. The surface morphology of the catalyst was characterized by FEI Nova SEM-450 scanning electron microscope (SEM) from Hong Kong Co., Ltd. Specific surface area and porosity adsorption (BET) were collected using an ASAP 2020 specific surface area and porosity analyzer from Micromeritics Company, USA, using N_2 as adsorbate and He as carrier gas, the samples were vacuum degassed at 90 °C for 8 h. The X-ray photoelectron spectroscopy (XPS) was carried out with ESCALAB 250Xi from Thermo Fisher Scientific Co., Ltd., and Al Kα (1486.6 eV) rays were used as the excitation source. The thermal stability of the catalyst was investigated by SDT Q-600 differential scanning calorimeter (DSC) from TA Instruments, USA, under N_2 atmosphere, with a flow rate of 100 mL min^{-1} and a heating rate of 10 °C min^{-1}.

Formic acid dehydrogenation

Formic acid dehydrogenation reactions were conducted in a 100 mL stainless steel autoclave with a magnetic stirrer to evaluate the catalytic activity of the Ni–Co–P/HAP in the decomposition of formic acid. Formic acid (HCOOH, 0.6086 g), catalyst (0.05 g) and isopropanol solvent (20 mL) were added to the autoclave, sealed the autoclave, and replaced the air in the autoclave with nitrogen (99.999%) three times. Heat to the

required temperature at a speed of 10 °C min^{-1}, and react for a period of time while stirring at a speed of 600 rpm. After the reaction, the autoclave was quickly cooled to room temperature, and the total volume of the H_2 and CO_2 products produced was measured. A gas chromatograph (SP-3420A) equipped with a thermal conductivity detector (TCD) and a hydrogen flame ionization detector (FID) was used to determine the gas and liquid products.

The HDO reaction of vanillin

Vanillin (2 mmol, 0.3043 g), formic acid (0.6086 g), catalyst (0.05 g) and 20 mL isopropanol were added to the autoclave. Seal the autoclave and replace the air in the autoclave with nitrogen (99.999%) three times. Heat to the required temperature at a speed of 10 °C min^{-1}, and react for a period of time while stirring at a speed of 600 rpm. After the reaction, it was cooled to room temperature. The product was quantitatively analyzed using high performance liquid chromatography (HPLC) from Waters, USA.

Results and discussion

Catalysts characterization

The XRD spectra of Ni–P, Ni–Co–P, Ni–Co–P/HAP and HAP are shown in Fig. 1. As can be seen from Fig. 1, the broad dispersion diffraction peaks of Ni–P and Ni–Co–P both appeared around at $2\theta = 45°$, which are the characteristic diffraction peaks of the amorphous alloy formed by metal Ni and metalloid P, indicating that the samples present the amorphous structure.[16,18] Compared with Ni–P amorphous alloys, the characteristic diffraction peaks of Ni–Co–P amorphous alloys are more dispersed around $2\theta = 45°$, which indicates that the introduction of Co is beneficial to the formation of amorphous structures. At the same time, compared with Ni–Co–P, the diffraction peak of Ni–Co–P/HAP near $2\theta = 45°$ was wider, and the peak intensity was obviously weakened, which indicates that Ni–Co–P amorphous alloy has been loaded on HAP.[19]

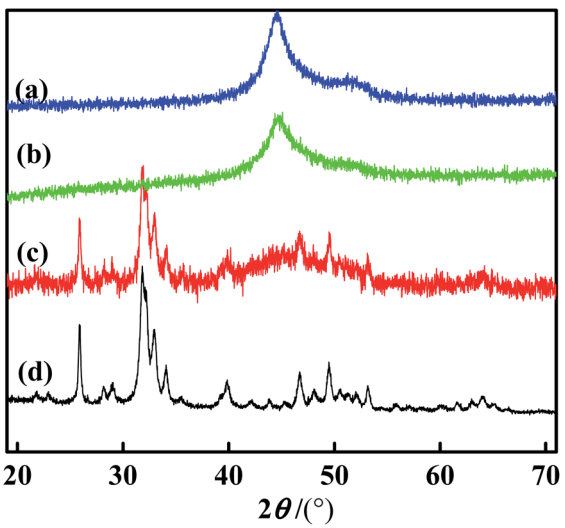

Fig. 1 XRD patterns of (a) Ni–P, (b) Ni–Co–P, (c) Ni–Co–P/HAP and (d) HAP.

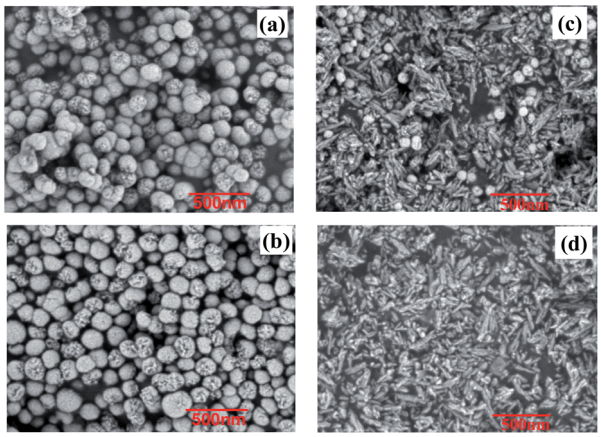

Fig. 2 SEM images of (a) Ni–P, (b) Ni–Co–P, (c) Ni–Co–P/HAP and (d) HAP.

The SEM of Ni–P, Ni–Co–P, Ni–Co–P/HAP and HAP are shown in Fig. 2. It can be seen from Fig. 2 that Ni–P and Ni–Co–P amorphous alloys were spherical particles with partial defects on the surface. The grain size of Ni–P amorphous alloy is not uniform, in the range of 100 to 200 nm, accompanied by a certain degree of agglomeration. By comparing with Ni–P, it can be seen that the particles of the Ni–Co–P and Ni–Co–P/HAP amorphous alloy modified by Co were relatively loose, which indicates that the agglomeration of amorphous alloy particles was effectively suppressed when the auxiliary Co was added during the preparation of catalyst. Comparing Fig. 2(c) and (d), it can be seen that the Ni–Co–P amorphous alloy forms spherical particles with a diameter of about 80 nm, which are dispersed on the HAP.

The BET results in Table 1 show that the specific surface areas of Ni–P and Ni–Co–P are basically the same, which is 8.28 and 7.97 $m^2\ g^{-1}$, respectively. The pore diameter of the amorphous alloys Ni–P and Ni–Co–P is 10.64 and 10.45 nm, respectively, the pore volume is 0.0282 and 0.0277 $cm^3\ g^{-1}$ respectively, which is also basically the same. Furthermore, HAP has a large specific surface area, pore size and pore volume, which is 65.94 $m^2\ g^{-1}$, 22.18 nm and 0.4036 $cm^3\ g^{-1}$, respectively, so HAP can be used as a good carrier for Ni–Co–P. When Ni–Co–P was loaded on HAP, the specific surface area of Ni–Co–P/HAP was reduced to 51.27 $m^2\ g^{-1}$, and the pore size and pore volume were reduced to 20.68 nm and 0.3372 $cm^3\ g^{-1}$,

Table 1 BET characterization results of Ni–P, Ni–Co–P, Ni–Co–P/HAP and HAP Samples

Catalyst	S_{BET}/$m^2\ g^{-1}$	Pore size/nm	Pore volume/$cm^3\ g^{-1}$
Ni–P	8.28	10.64	0.0282
Ni–Co–P	7.97	10.45	0.0277
Ni–Co–P/HAP	51.27	20.68	0.3372
HAP	65.94	22.18	0.4036

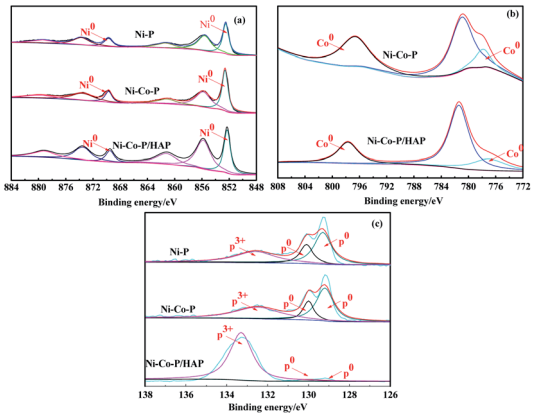

Fig. 3 XPS spectra of Ni 2p, Co 2p and P 2p of Ni–P, Ni–Co–P and Ni–Co–P/HAP samples (a) Ni 2p (b) Co 2p and (c) P 2p.

respectively, which shows that Ni–Co–P was successfully loaded on HAP.

The XPS spectra of Ni 2p, Co 2p and P 2p of Ni–P, Ni–Co–P and Ni–Co–P/HAP amorphous alloys are shown in Fig. 3. It can be seen from Fig. 3(a) that the Ni 2p of the three amorphous alloys all appeared six peaks near 852, 855, 861, 869, 873 and 879 eV, among which the peaks near 852, 869 eV were attributed to Ni^0, and the remaining peaks are attributed to Ni^{2+}. The oxidation state of Ni may originate from the NiO formed during the preparation of the catalyst,[20–22] and the presence of NiO can catalyze the decomposition of formic acid.[23,24] The rapid decomposition of formic acid is beneficial to the hydrodeoxygenation of vanillin. The XPS of the three catalysts Co 2p is shown in Fig. 3(b). It can be seen that the peaks of Co^0 in Co 2p appear about 777 and 796 eV. The XPS spectrum of P 2p is shown in Fig. 3(c), in terms of Ni–P, Ni–Co–P and Ni–Co–P/HAP, the peaks of P^0 appear around 129 and 130 eV, while the peaks near 132 eV were attributed to P^{3+}, which is derived from $H_2PO_3^-$ generated during the preparation process.[25,26] In addition, the peak height of P^0 in Ni–Co–P/HAP was sharply decreased compared with the p^0 of Ni–P and Ni–Co–P, which is because there is a strong and broad peak attributable to P^{3+} in HAP. According to related reports, the standard binding energies (BEs) of Ni^0 are 853.0 and 869.9 eV, and the BEs of Co^0 are 777.8 eV and 796.7 ev.[21,27] It can be seen that the BEs of Ni^0, Co^0 of the catalysts were decreased, compared with the standard BEs, which indicates that the electrons have been transferred, that is, electrons are transferred from P to Ni, which result in the Ni of catalyst in an electron-rich state. According to relevant literature reports that the electron-rich Ni exhibits an excellent ability in adsorbing hydrogen and can better activate hydrogen, which is beneficial to the hydrogenation reaction.[28]

The DSC curves of Ni–P, Ni–Co–P and Ni–Co–P/HAP are shown in Fig. 4. It can be seen from Fig. 4 that Ni–P and Ni–Co–P amorphous alloys appeared exothermic peaks near 365 °C and 402 °C, respectively, which are typical crystallization exothermic peaks of amorphous alloys. Compared with Ni–P amorphous alloy, the crystallization temperature of Ni–Co–P amorphous alloy was significantly higher, which indicates that the introduction of Co can improve the thermal stability of the amorphous structure. Comparing the DSC curves of Ni–Co–P and Ni–Co–P/HAP, it can be seen that Ni–Co–P/HAP has higher thermal stability, which is also the key to the better catalytic performance of the Ni–Co–P/HAP in the HDO reaction of vanillin. Meanwhile, it can be seen from the SEM characterization (Fig. 2(c)) that the Ni–Co–P amorphous alloy supported on HAP is beneficial to the dispersion of the Ni–Co–P amorphous alloy catalyst, which can effectively prevent the agglomeration or crystallization of amorphous alloys. This is also the main reason why the stability of Ni–Co–P/HAP amorphous alloy was significantly improved compared with Ni–P and Ni–Co–P.[29]

Decomposition of formic acid

Under the reaction conditions of 20 mL isopropanol, 0.6086 g formic acid, 0.05 g catalyst, and reaction temperature of 190 °C,

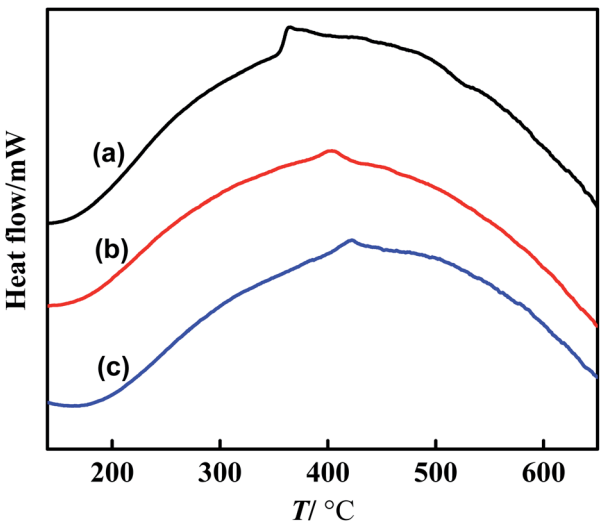

Fig. 4 DSC curves of (a) Ni–P, (b) Ni–Co–P and (c) Ni–Co–P/HAP.

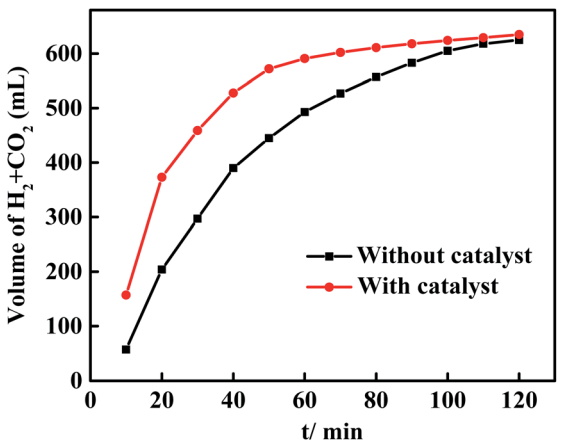

Fig. 5 Catalytic decomposition of formic acid with Ni–Co–P/HAP catalyst.

Table 2 The HDO reaction of vanillin catalyzed by different catalysts[a]

Catalyst	$X_{vanillin}$ (%)	S_{MMP} (%)	S_{HMP} (%)
None	<1	None	None
HAP	<1	None	None
Ni–P	76.88	50.41	16.22
Ni–Co–P	82.96	61.72	7.32
Ni–Co–P/HAP	84.23	65.36	6.42

[a] Reaction conditions: 2 mmol vanillin, catalyst 0.05 g, solvent 20 mL isopropanol, *m*(formic acid) : *m*(vanillin) = 2 : 1, 190 °C, 3 h.

the catalytic performance of Ni–Co–P/HAP amorphous alloy for the decomposition of formic acid was investigated. The result is shown in Fig. 5, in the absence of a catalyst, the total volume of H_2 and CO_2 (625 mL) remained unchanged after 100 minutes of formic acid decomposition reaction. The rate of formic acid dehydrogenation was increased significantly after introducing the catalyst into the reaction system. The dehydrogenation of formic acid was completed when the reaction time reaches 70 minutes, the reason is that the decomposition of formic acid can be catalyzed effectively by Ni–Co–P/HAP amorphous alloy catalyst, which is consistent with the previous reports.[18,30] In addition, acetone are usually produced as by-products in the reaction system when isopropanol as a hydrogen source. Formic acid can release hydrogen through the dehydrogenation reaction (HCOOH → H_2 + CO_2), and the process is usually accompanied by an undesirable dehydration pathway (HCOOH → H_2O + CO). However, CO and acetone were not detected by gas chromatography, which confirms that formic acid was the main hydrogen source of the reaction and no side reactions occurred in the dehydrogenation reaction of formic acid, while isopropanol was only used as a solvent in the hydrogenation reaction of vanillin.[19,31] In addition, the maximum total volume of H_2 and CO_2 produced by the decomposition of formic acid is 635 mL, and the conversion of formic acid is calculated at 98.16%.

Evaluation of the activity of the HDO reaction of vanillin

The HDO reaction of vanillin was chosen as a model reaction to investigate the catalytic performance of catalysts. The effect of the catalyst on the HDO reaction of vanillin is shown in Table 2. It can be seen from Table 2 that the HDO reaction of vanillin cannot proceed when no catalyst was added or only carrier HAP was added. The activity of the catalyst was significantly improved when using Ni–P amorphous alloy as the catalyst, and the conversion of vanillin reached 76.88%, accompanied by 50.41% MMP and 16.22% vanillin alcohol (HMP) selectivity. Compared with Ni–P, the selectivity of MMP was increased to 61.72% when using Ni–Co–P amorphous

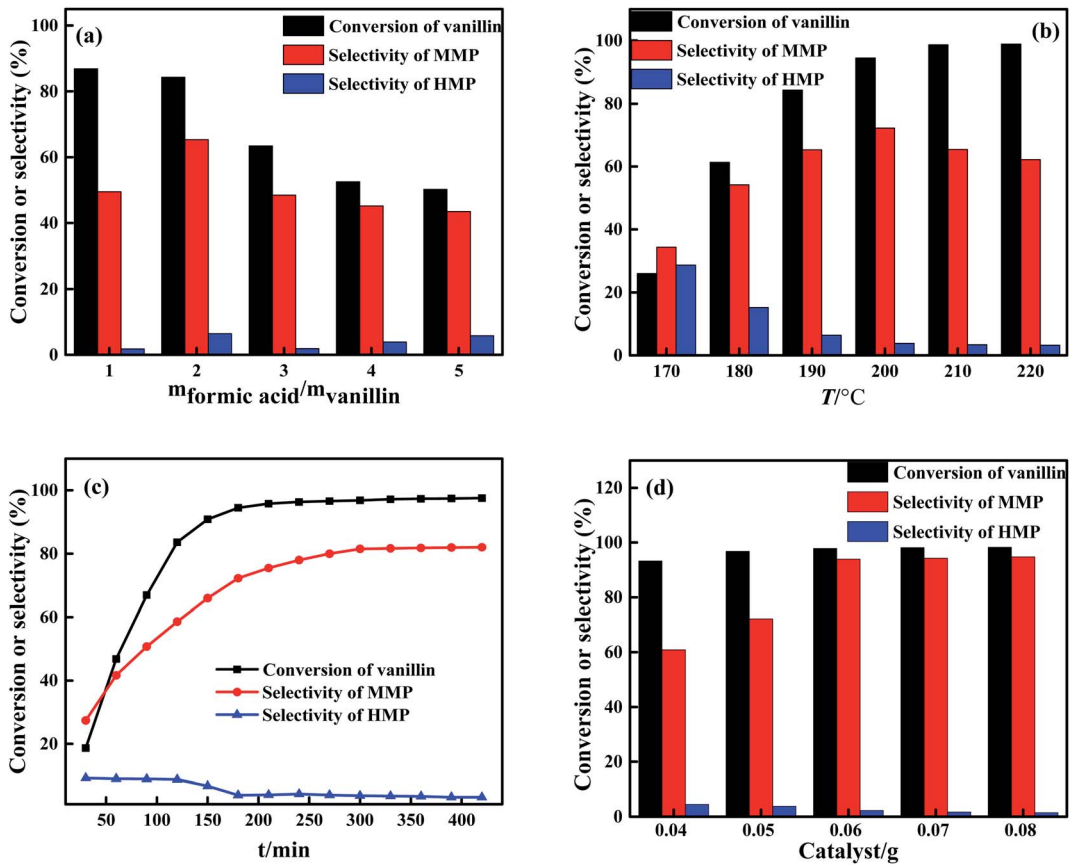

Fig. 6 Influence of (a) formic acid amount (b) reaction temperature (c) reaction time and (d) catalyst amount on vanillin HDO reaction.

alloy as the catalyst, and the selectivity of HMP was decreased to 7.32%, which indicates that the introduction of Co can improve the activity and selectivity of the catalyst, and promote the hydrogenation of HMP to MMP. Meanwhile, the activity of the catalyst was slightly increased, the selectivity of HMP was further reduced, while the selectivity of MMP was increased to 65.36% when using Ni–Co–P/HAP amorphous alloy as the catalyst. This is because the Ni–Co–P amorphous alloy was uniformly dispersed, the agglomeration of the catalyst was reduced and the stability of the catalyst was improved when Ni–Co–P was loaded on the HAP, thereby the activity of the catalyst was increased.

The effect of the amount of formic acid, reaction temperature, reaction time and the amount of catalyst on the HDO reaction of vanillin were investigated, the results were shown in Fig. 6. Here, the effect of the amount of formic acid on the vanillin HDO reaction was shown in Fig. 6(a), under the reaction conditions of 2 mmol vanillin, 0.05 g catalyst, 20 mL isopropanol, 190 °C and 3 h. It can be seen from Fig. 6(a) that in the initial stage of the reaction, due to the small amount of formic acid in the system, the decomposition of formic acid cannot provide sufficient hydrogen, and HMP cannot be hydrogenated in time to generate MMP, resulting in the side reaction of aldol condensation,[32,33] and the selectivity of the product MMP was 49.55%. As the amount of formic acid increases, the hydrogen source in the reaction system increased, the selectivity of MMP was increased significantly. The highest selectivity of product MMP was 65.36% when m(formic acid) : m(vanillin) = 2 : 1. When the amount of formic acid was further increased, the selectivity of MMP was decreased. This is because hydrogen protons will combine with formic acid to generate carbocations when there is too much formic acid in the reaction system, which intensifies the occurrence of HMP coupling side reactions.[33] Fig. 6(b) presents the effect of reaction temperature on the HDO reactions of vanillin under the reaction conditions of 2 mmol vanillin, 0.05 g catalyst, 20 mL isopropanol, m(formic acid) : m(vanillin) = 2 : 1 and 3 h. As shown in Fig. 6(b), the best results were achieved under 200 °C, which showed a 94.48% conversion of vanillin and 72.22% selectivity of MMP. When the temperature further increased, although the conversion of vanillin slightly increased, the selectivity of the product MMP was significantly decreased. The reason is that the HDO reaction of vanillin is an exothermic reaction, but formic acid decomposition to H_2 is an endothermic reaction, the rise of temperature is beneficial to the decomposition of formic acid to produce hydrogen, but the too high temperature will cause the coupling reaction of MMP which the selectivity of MMP was decreased.[34]

In addition, under the reaction conditions of 2 mmol vanillin, 0.05 g catalyst, 20 mL isopropanol, m(formic acid) : m(vanillin) = 2 : 1 and 200 °C, the effect of the reaction time on the vanillin HDO reaction was investigated. It can be seen from Fig. 6(c) that in the initial reaction stage, the reaction proceeded slowly and the reaction was incomplete. As the reaction time increases, the conversion of vanillin and the selectivity of the product MMP was increased gradually. Vanillin was almost completely converted at 300 min, the conversion rate of vanillin was 96.79%, the selectivity of the target product MMP was 81.47%, and they remained unchanged as the reaction time was further increased. Fig. 6(d) shows the effect of the amount of Ni–Co–P/HAP amorphous alloy catalyst on the vanillin HDO reaction under the reaction conditions of 2 mmol vanillin, 20 mL isopropanol, m(formic acid) : m(vanillin) = 2 : 1, 200 °C and 300 min. It can be seen from Fig. 6(d) that the conversion of vanillin was increased slightly from 93.28% to 97.86%, while the selectivity of MMP was increased significantly from 60.89% to 93.97% when the increase of the amount of Ni–Co–P/HAP catalyst from 0.04 g to 0.06 g. This is because the Ni–Co–P/HAP amorphous alloy plays a dual role in the HDO reaction of vanillin: on the one hand, the NiO component in Ni–Co–P/HAP has the function of catalyzing the decomposition of formic acid to obtain H_2; on the other hand, Ni–Co–P/HAP can promote the HDO reaction of vanillin. Therefore, the active component of the catalyst is less than enough to catalyze the decomposition of formic acid and the vanillin HDO reaction when the amount of the catalyst is too small, the formic acid cannot provide a sufficient hydrogen source for the vanillin HDO, which leads to low selectivity of the MMP.

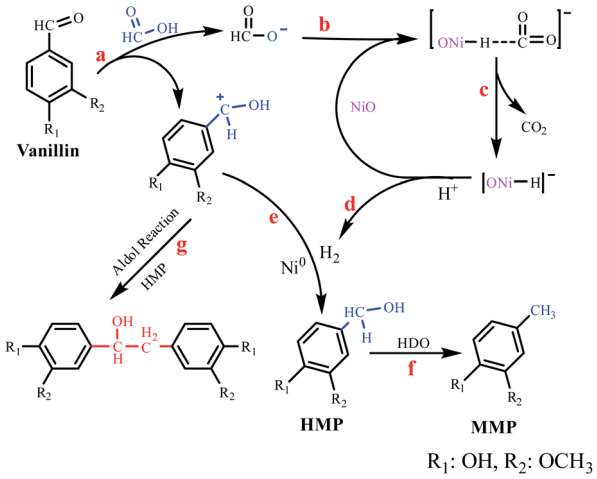

Fig. 7 Mechanism proposed for the HDO reaction of vanillin using formic acid as the hydrogen source.

Mechanism study

Based on experimental studies and literature reports, a plausible reaction mechanism for the HDO reaction of vanillin with formic acid as a hydrogen source has been proposed (Fig. 7).[35–37] First, formic acid can generate hydrogen protons, the carbonyl group can be activated by hydrogen protons to form carbocations (Fig. 7, reaction a), and the carbocations undergoes condensation side reactions with HMP, which is not conducive to the further hydrogenation of HMP to produce MMP, which is also the main reason why the selectivity of the product MMP was decreased a when there is too much formic acid in the reaction system. Secondly, formate decomposes on the surface of NiO to form CO_2 and $[ONi–H]^-$ intermediates (Fig. 7, reactions b and c), $[ONi–H]^-$ intermediates combine with H^+ ions to

form H_2 and NiO (Fig. 7, reaction d), at this time, the NiO catalytic cycle is completed, returning to the initial state.[38] The H_2 generated by the decomposition of formic acid was activated by Ni^0 and hydrogenated with vanillin to form HMP (Fig. 7, reaction e), and HMP was further hydrogenated to form MMP (Fig. 7, reaction f).[39,40] The experimental results showed that the condensation reaction could be greatly reduced (Fig. 7, reaction g) when the hydrogenation reaction proceeded rapidly (Fig. 7, reaction e and f). Under the premise that hydrogenation and condensation are competing reactions, improving the hydrogenation efficiency is an effective way to reduce condensation side reactions.[41,42]

Conclusions

Herein, the Ni–Co–P/HAP amorphous alloy catalyst was synthesized by impregnation-chemical reduction method, and it exhibits good catalytic activity for *in situ* HDO reaction of vanillin with formic acid as the hydrogen source. The conversion of vanillin could be high to 97.86% with MMP selectivity of 93.97%, under optimized reaction conditions of 2 mmol vanillin, 0.06 g catalyst, 20 mL isopropanol solvent, *m*(formic acid) : *m*(vanillin) = 2 : 1, 200 °C and 300 min. Ni–Co–P/HAP, as a dual-function catalyst, can promote the decomposition of formic acid and catalyze the *in situ* HDO reaction of vanillin, which provides a new catalytic way for the hydrogenation of biomass using formic acid as a hydrogen source. Mechanism studies have shown that the rapid hydrogenation of carbocations and HMP can effectively reduce the occurrence of condensation side reactions, which is the key to further improving the selectivity of the target product MMP.

Conflicts of interest

The authors declare no conflicts of interest.

Acknowledgements

This work was financially supported by the Natural Science Foundation of Hebei Province (No. B2018202293).

References

1 M. Saidi, F. Samimi, D. Karimipourfard, T. Nimmanwudipong, B. C. Gates and M. R. Rahimpour, *Energy Environ. Sci.*, 2014, **7**, 103–129.
2 X. Li, G. Chen, C. Liu, W. Ma, B. Yan and J. Zhang, *Renewable Sustainable Energy Rev.*, 2017, **71**, 296–308.
3 P. R. Patwardhan, R. C. Brown and B. H. Shanks, *ChemSusChem*, 2011, **4**, 1629–1636.
4 Y. Y. Wang, L. L. Ling and H. Jiang, *Green Chem.*, 2016, **18**, 4032–4041.
5 H. Jiang, *J. Chem. Res.*, 2019, **37**, 761–763.
6 F. Huang, W. Li, Q. Lu and X. Zhu, *Chem. Eng. Technol.*, 2010, **33**, 2082–2088.
7 J. Du, J. Zhang, Y. Sun, W. Jia, Z. Si, H. Gao and L. Lin, *J. Catal.*, 2018, **368**, 69–78.
8 D. A. Bulushev, S. Beloshapkin, P. E. Plyusnin, Y. V. Shubin, V. I. Bukhtiyarov, S. V. Korenev and J. R. Ross, *J. Catal.*, 2013, **299**, 171–180.
9 M. Grasemann and G. Laurenczy, *Energy Environ. Sci.*, 2012, **5**, 8171–8181.
10 C. Hu, J. K. Pulleri, S. W. Ting and K. Y. Chan, *Int. J. Hydrogen Energy*, 2014, **39**, 381–390.
11 M. O. Bengoechea, A. Hertzberg, N. Miletić, P. L. Arias and T. Barth, *J. Anal. Appl. Pyrolysis*, 2015, **113**, 713–722.
12 C. Pu, J. Zhang, G. Chang, Y. Xiao, X. Ma, J. Wu and X. Yang, *Carbon*, 2020, **159**, 451–460.
13 L. Wang, B. Zhang, X. Meng, D. S. Su and F. S. Xiao, *ChemSusChem*, 2014, **7**, 1537–1541.
14 R. Nie, X. Peng, H. Zhang, X. Yu, X. Lu, D. Zhou and Q. Xia, *Catal. Sci. Technol.*, 2017, **7**, 627–634.
15 A. Jia, X. Yao, L. Feng, Z. Ma, F. Li and Y. Wang, *Eur. J. Inorg. Chem.*, 2020, **13**, 1184–1191.
16 W. Wang, Y. Yang, H. Luo and W. Liu, *React. Kinet., Mech. Catal.*, 2010, **101**, 105–115.
17 F. Brandi, M. Bäumel, V. Molinari, I. Shekova, I. Lauermann, T. Heil and M. Al-Naji, *Green Chem.*, 2020, **22**, 2755–2766.
18 M. H. Qiao, S. H. Xie, W. L. Dai and J. F. Deng, *Catal. Lett.*, 2001, **71**, 187–192.
19 G. Xie, W. Sun and W. Li, *Catal. Commun.*, 2008, **10**, 333–335.
20 M. H. Lin, B. Zhao and Y. W. Chen, *Ind. Eng. Chem. Res.*, 2009, **48**, 7037–7043.
21 J. Legrand, A. Taleb, S. Gota, M. J. Guittet and C. Petit, *Langmuir*, 2002, **18**, 4131–4137.
22 L. Wang, W. Liu and X. Wang, *Tribol. Lett.*, 2009, **37**, 381–387.
23 W. Zhao, A. D. Doyle, S. E. Morgan, M. Bajdich, J. K. Nørskov and C. T. Campbell, *J. Phys. Chem. C*, 2017, **121**, 28001–28006.
24 T. M. Huynh, U. Armbruster, M. M. Pohl, M. Schneider, J. Radnik, D. L. Hoang and A. Martin, *ChemCatChem*, 2014, **6**, 1940–1951.
25 Z. Zhu, J. Ma, L. Xu, L. Xu, H. Li and H. Li, *ACS Catal.*, 2012, **2**, 2119–2125.
26 J. H. Shen and Y. W. Chen, *J. Mol. Catal. A: Chem.*, 2007, **273**, 265–276.
27 Z. Li, H. Li, L. Wang, T. Liu, T. Zhang, G. Wang and G. Xie, *Int. J. Hydrogen Energy*, 2014, **39**, 14935–14941.
28 W. Y. Wang, Y. Q. Yang, J. G. Bao and H. A. Luo, *Catal. Commun.*, 2009, **11**, 100–105.
29 F. Li, J. Liang, K. Wang, B. Cao, W. Zhu and H. Song, *Can. J. Chem. Eng.*, 2017, **95**, 2012–2017.
30 W. Wang, Y. Yang, H. Luo, H. Peng, B. He and W. Liu, *Catal. Commun.*, 2011, **12**, 1275–1279.
31 J. Reyes, E. Arriola, J. A. Hernández and G. A. Fuentes, *Appl. Catal., A*, 2015, **497**, 211–215.
32 L. Zhang, Z. Xin, Z. Liu, G. Wei, Z. Li and Y. Ou, *Renewable Energy*, 2020, **147**, 695–704.
33 R. Fan, C. Chen, M. Han, W. Gong, H. Zhang, Y. Zhang and G. Wang, *Small*, 2018, **14**, 1801953.
34 M. J. Hidajat, A. Riaz and J. Kim, *Chem. Eng. J.*, 2018, **348**, 799–810.
35 K. Mori, T. Taga and H. Yamashita, *ACS Catal.*, 2017, **7**, 3147–3151.

36 K. Tedsree, T. Li, S. Jones, C. W. A. Chan, K. M. K. Yu, P. A. Bagot and S. C. E. Tsang, *Nat. Nanotechnol.*, 2011, **6**, 302–307.
37 M. Al-Naji, M. Popova, Z. Chen, N. Wilde and R. Gläser, *ACS Sustainable Chem. Eng.*, 2019, **8**, 393–402.
38 K. Mori, M. Dojo and H. Yamashita, *ACS Catal.*, 2013, **3**, 1114–1119.
39 O. Kikhtyanin, L. Čapek, Z. Tišler, R. Velvarská, A. Panasewicz, P. Diblíková and D. Kubička, *Front. Chem.*, 2018, **6**, 176.
40 N. C. Ellebracht and C. W. Jones, *Carbohydr. Polym.*, 2020, **233**, 115825.
41 S. Zhou, F. Dai, C. Dang, M. Wang, D. Liu, F. Lu and H. Qi, *Green Chem.*, 2019, **21**, 4732–4747.
42 V. R. Bakuru, D. Davis and S. B. Kalidindi, *Dalton Trans.*, 2019, **48**, 8573–8577.